Pure appl. geophys. 164 (2007) 325–353
0033–4553/07/030325–29
DOI 10.1007/s00024-006-0181-4

Pure and Applied Geophysics

Seismic Records of the 2004 Sumatra and Other Tsunamis: A Quantitative Study

Emile A. Okal

Abstract—Following the recent reports by Yuan *et al.* (2005) of recordings of the 2004 Sumatra tsunami on the horizontal components of coastal seismometers in the Indian Ocean basin, we build a much enhanced dataset extending into the Atlantic and Pacific Oceans, as far away as Bermuda and Hawaii, and also expanded to five additional events in the years 1995–2006. In order to interpret these records quantitatively, we propose that the instruments are responding to the combination of horizontal displacement, tilt and perturbation in gravity described by Gilbert (1980), and induced by the passage of the progressive tsunami wave over the ocean basin. In this crude approximation, we simply ignore the island or continent structure, and assume that the seismometer functions *de facto* as an ocean-bottom instrument. The records can then be interpreted in the framework of tsunami normal mode theory,and lead to acceptable estimates of the seismic moment of the parent earthquakes. We further demonstrate the feasibility of deconvolving the response of the ocean floor in order to reconstruct the time series of the tsunami wave height at the surface of the ocean, suggesting that island or coastal continental seismometers could complement the function of tsunameters.

Key words: Tsunami, seismic recording, 2004 Sumatra earthquake.

Introduction

In the aftermath of the 2004 Sumatra tsunami, Yuan *et al.* (2005) reported that seven seismic stations located on islands and continental shores of the Indian Ocean had recorded on their horizontal components the actual impact of the tsunami on the nearby shores. These signals were generally polarized perpendicular to the shoreline and featured energy in the 1 to 2 mHz range and amplitudes, expressed as accelerations, on the order of 10^{-4} cm/s^2. Following the landslides at Stromboli in 2002, La Rocca *et al.* (2004) had similarly reported low-frequency signals at the seismic station on the nearby island of Panarea (21 km away from the source), but Yuan *et al.*'s remarkable observations constitute the first such report in the far field. They were also briefly confirmed by Hanson and Bowman (2005).

Department of Geological Sciences, Northwestern University, Evanston, IL 60201, USA.

In this context, the purpose of the present paper is to expand on YUAN *et al.*'s (2005) work in several directions, by showing that such recordings were detectable worldwide; that the signals extend, at least in the regional field, to high frequencies in the 10 mHz range; that such signals are justifiable quantitatively using normal mode theory; that similar signals from smaller tsunamis are also identifiable in the seismic record, with their spectral amplitudes correlating well with the seismic moment of the parent earthquake; that acceptable time series of the tsunami on the high seas can be reconstructed from seismic records; and finally that seismic records of tsunami waves can also be obtained on vertical seismometers, albeit at a lower amplitude.

2. The Universal Character of the Seismic Recordings

Following in the footsteps of YUAN *et al.* (2005), we conducted a systematic worldwide search for similar records, including at stations located outside the Indian Ocean. At each targeted station, we extracted the long-period horizontal channels, and proceeded to deconvolve the instrument and bandpass filter the resulting ground motion between 0.1 and 10 mHz. Table 1 lists the stations at which the tsunami was detected, with relevant information such as dominant frequency and equivalent amplitude; their location is shown on Figure 1. Figure 2 provides representative examples of typical time series, after deconvolution of the instrument response to ground displacement and bandpass filtering in the 0.1–10 mHz range. The association of the signals with the tsunami was made on the basis of its arrival time, as predicted by the global simulation of TITOV *et al.* (2005). Among the most remarkable results, we note that the tsunami is well recorded seismically as far as Bermuda (29 hours after origin time and at a distance of 20,800 km around the Cape of Good Hope), and Kipapa, Hawaii (31.5 hours after origin time). The latter site is reached after a westward path estimated at 26,700 km, through the Atlantic Ocean and the Drake Passage (the eastward path going south of Australia being about 8 hours shorter). This is an expression of the strong directivity of the source towards the Western Indian Ocean, at right angles to the direction of faulting (BEN-MENAHEM and ROSENMAN, 1972), and of the efficient focusing of the wave by the shallow bathymetry along the Southwest Indian Ridge (TITOV *et al.*, 2005) as previously observed for Pacific Ocean tsunamis by WOODS and OKAL (1987) and SATAKE (1988). These effects also probably contribute to the spectacular quality of the recording at Hope, South Georgia, where the tsunami is clearly discernible on the raw record, without the need for filtering or instrument deconvolution (Fig. 3); they may be compounded by local resonance effects in the Bays of Cumberland. The tsunami is also well recorded at station SBA (Scott Base, Antarctica), following a somewhat convoluted path around Australia and into McMurdo Sound.

Table 1

List and properties of seismic records of the 2004 Sumatra tsunami

Station		Epicentral distance (km)	Distance from shore (km)	Arrival date and time	Spectral peak			Peak-to-peak amplitude (cm)		
Code	Location				Prominent component	Amplitude (cm*s)	Period (s)	Apparent ground motion	Deconvolved η	Virtual gauge (Titov *et al.*, 2005)
COCO	Cocos Island, IOTA	1721	< 1		N141E			20	210	46
DGAR	Diego Garcia, BIOT	2748	< 1	(361) 04:40	EW	3500	800	14	370	135
MSEY	Mahé, Seychelles	4564	2; 120 ¶¶	(361) 08:00	N247E	700	800	6.3	133	42
AIS	Ile Amsterdam, TAAF	4930	< 4	(361) 07:48	EW	2000	800	4	170	54
RER	Rivière de l'Est, Réunion	5133	7	(361) 07:46	EW	17000	3000	1.6	42	45
PAF	Port-aux-Français, Kerguelen, TAAF	6340	< 2; 20 †	(361) 10:20	NS	5500	1000	7	186	93
CRZF	Ile de la Possession, Crozet, TAAF	7009	< 2	(361) 10:50	EW	2700	800	18	107	36
CASY	Casey, Antarctica	7818	< 1	(361) 12:18	NS	4000	800	10	208	99
DRV	Dumont d'Urville, Antarctica	8519	< 1; 30 ¶	(361) 14:24	NS	1000	800	4	43	40
HOPE	Hope, South Georgia	12906	< 1; 8 †	(361) 20:07	NS	6000	800	13	291	15
TRIS	Edinburgh, Tristan da Cunha, BOT	9700 (*)	< 1	(361) 14:13	EW	18000	3000	21	31	10
SBA	Scott Base, Antarctica	11300 (*)		(361) 19:02	NS	500	800	1.5	27	7
DZM	Dzoumac, New Caledonia	12000 (*)	15	(361) 20:29	NS	3500	950	9	127	4.5
ASCN	Ascension Island, BOT	13900 (*)	3	(362) 00:48	NS	10000	3000	3	10	8.5
BBSR	Hamilton, Bermuda	20800(*)	4	(362) 05:52	N126E	2200	1500	0.6	16	2.5
KIP	Kipapa, Hawaii, USA	26700 (*)	10	(362) 08:33	NS	7000	3000	0.5	10	1.5

(*) Distances to these stations are estimated along a path deviating from the great circle in order to avoid continental masses. Consequently, they are not used in the source retrieval computations.

† For stations located in strongly indented bays, we give the distance to the nearest shore point followed by the distance to a more regular coastline.

¶ For stations involving a broad continental shelf, we give first the distance to the nearest shoreline, and then to the continental slope.

BIOT: British Indian Ocean Territory; BOT: British Overseas Territory; IOTA: Indian Ocean Territories of Australia; TAAF: Terres Australes et Antarctiques Françaises.

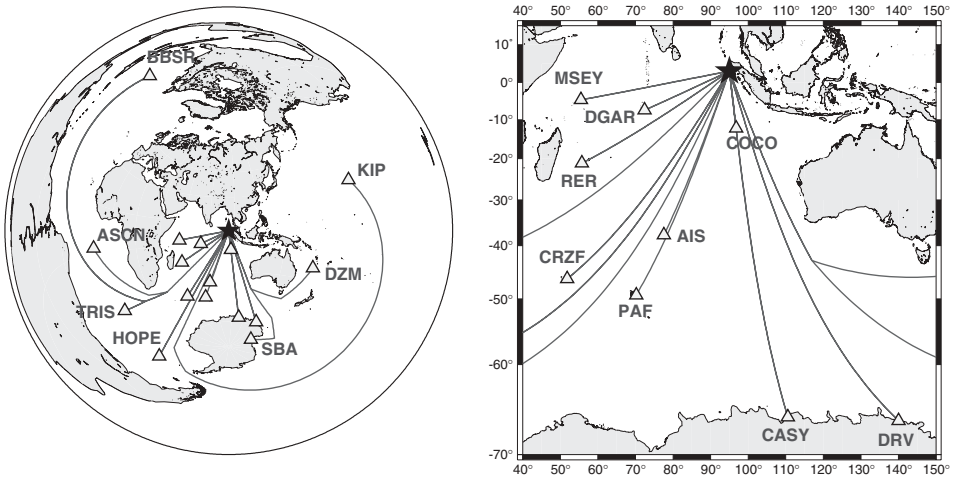

Figure 1
Maps of seismic stations (triangles) having recorded the 2004 Sumatra tsunami. *Left*: Azimuthal equidistant projection centered on the epicenter of the earthquake (star). Segmented lines correspond to paths departing from great circles to avoid continental masses. *Right*: Mercator projection close-up of the Indian Ocean Basin.

As a whole, we were able to make observations at 16 stations, including nine not described by YUAN *et al.* (2005). Of the latter, two are in the Indian Ocean Basin (MSEY and DRV), four in the Atlantic (HOPE, TRIS, ASCN and BBSR), and three in the Pacific (DZM, SBA and KIP). By contrast, we failed to observe detectable signals at the stations listed in Table 2. We confirm the observation by YUAN *et al.* (2005) that only coastal stations can record seismic signals of impacting tsunamis. This is best demonstrated by the case of the two Hawaiian stations: the tsunami is recorded at KIP on Oahu, only 10 km from the coastline, while it is not at POHA, on the saddle of the Big Island, 55 km from the receiving shore. An examination of the datasets of Tables 1 and 2 suggests an empirical threshold of ˜35 km for the detection of the Indonesian tsunami in both the near and far fields. In addition, a station deployed near the shore at the toe of a large gulf or bay (e.g., Arta Grotte, Djibouti) may not record the tsunami; furthermore, in the presence of an extended continental shelf, even a coastal station (e.g., Montagne des Pères, French Guyana, only 10 km from the shore) will not record the tsunami. The absence of record at Rarotonga (less than 3 km from the shore line) probably reflects the low amplitude of the wavefield in that part of the Central Pacific, but the situation at Easter Island (RPN) is more intriguing, since the stations lies practically on the path to KIP, where the tsunami is well recorded.

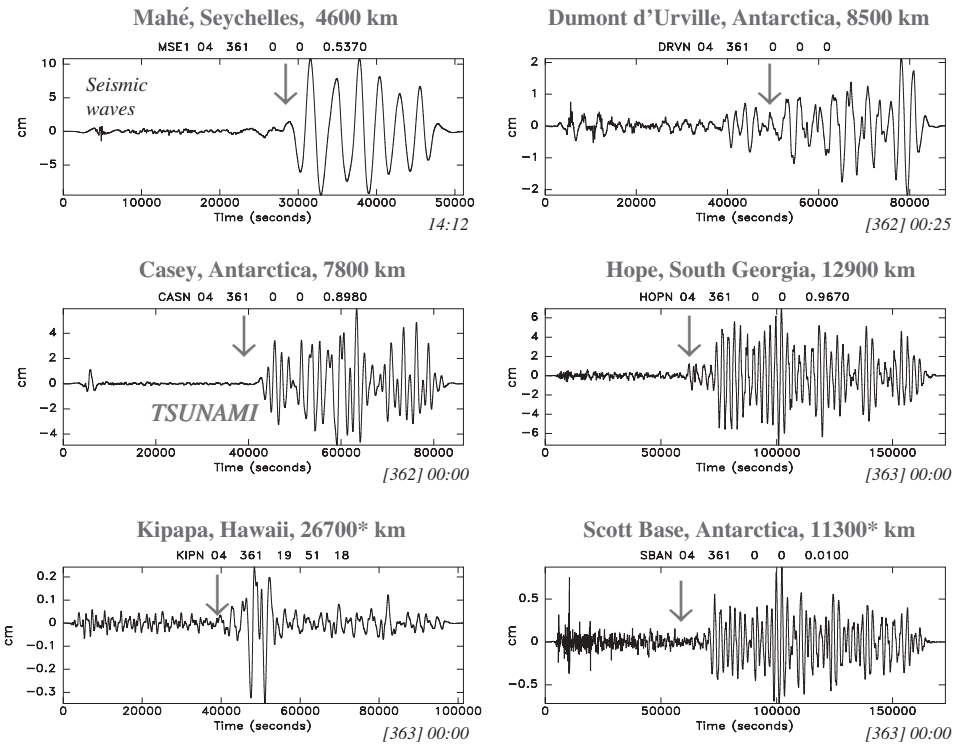

Figure 2
Representative examples of seismic recordings of the 2004 Sumatra tsunami. On each frame, the instrument response was deconvolved, and the record bandpass filtered, to obtain the equivalent ground motion between 0.1 and 10 mHz. Note the different time and displacement scales on each frame. All records start at 00:00 UTC (except KIP; 19:51 UTC), on 26 December 2004. The numbers in italics at the bottom right of each frame show the time at the end of each record (including Julian Day in brackets). The vertical arrows point to the arrival time of the tsunami, computed along the great circle to the station or, at Kipapa and Scott Base, using an estimated distance around continental masses (flagged by a star, as in Table 1).

3. High-frequency Components of the Tsunami

On Figure 4, we document that energy is present on the seismic record of the tsunami at Amsterdam Island (AIS) at the higher frequencies detected on hydrophones by HANSON and BOWMAN (2005) and OKAL *et al.* (2007). These spectral components, which fall outside the range of conventional observations of tsunamis, are characterized by significant dispersion, as they do not follow the shallow-water approximation. Rather, the black solid line on Figure 4 shows the group arrival times predicted by the classical dispersion relation

$$\omega^2 = g\ k \cdot \tanh\ (kH) \qquad (1)$$

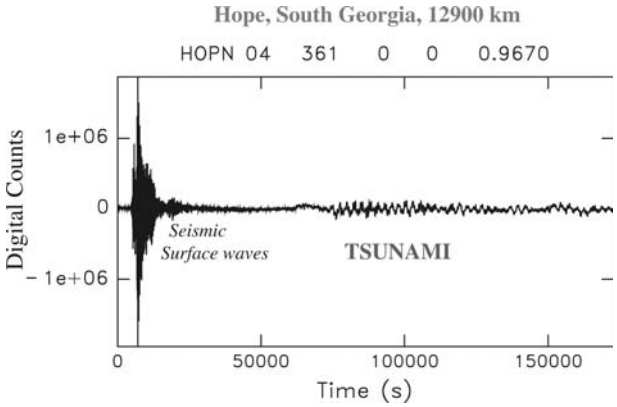

Figure 3
Original North-South Long-Period (LHN) record at Hope, South Georgia. This unprocessed raw seismogram starts at 00:00 UTC on 26 December and lasts 48 hours. Note the clear recording of the tsunami.

Table 2

Seismic stations at which the 2004 Sumatra tsunami was not detectable

Code	Location	Distance (km) from		
		Shore	high seas (†)	continental slope (¶)
ATD	Arta Grotte, Djibouti	7	60	
EFI	East Falklands, Falkland Is.	25		45
MPG	Montagne des Pères, French Guyana	10		135
NWA	Narrogin, Western Australia	150		
PALK	Pallekele, Sri Lanka	120		
POHA	Pohakuloa, Hawaii, USA	55		
RAR	Rarotonga, Cook Islands	< 3		
RPN	RapaNui, Easter Island, Chile	3		
TAU	Hobart, Tasmania, Australia	3	45	75

The symbols (†; ¶) refer to the conventions of Table 1.

between angular frequency ω, acceleration of gravity g and wave number k, for an average basin depth $H = 4$ km, and using the epicentral parameters (3.30°N; 95.98°E; origin time 00:58:50 UT) corresponding to the nucleation of the rupture; the white line uses an average depth of 3.5 km, and a centroid of rupture at 7°N, 93°E, with an origin time of 01:03:00 UT. At each frequency, the first arrival of tsunami energy at AIS coincides with the former, and the maximum of energy generally

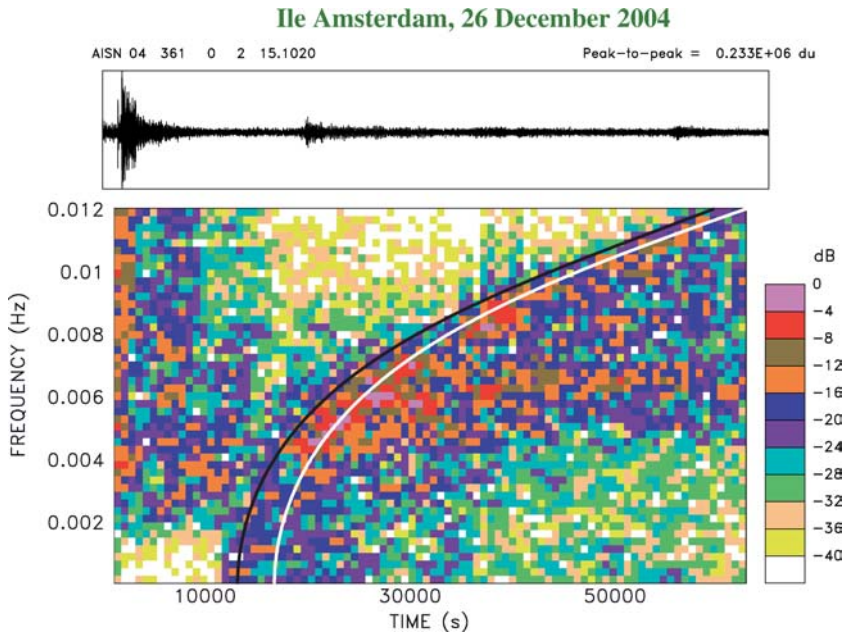

Figure 4
Spectrogram of the tsunami recording at AIS (Ile Amsterdam). The individual pixels identify the spectral amplitude present in the wave train as a function of time (abscissa) and frequency (ordinate), according to the logarithmic scale at right. In order to emphasize the high frequencies in the record, we processed the raw seismogram, without deconvolution of the instrument response. The black curve is the dispersion expected from equation (1) for a 4-km deep ocean basin and a source at the epicenter of rupture. The white curve uses a 3.5-km basin and places the source at the centroid of rupture (Tsai *et al.*, 2005).

follows the latter. The signals then last for many hours. High-frequency components of the tsunami wave are of particular concern in the framework of civil defense as Okal *et al.* (2006a,b) have suggested that they are responsible for setting distant harbors in resonance long after the passage of the main wavetrains observed at lower frequencies.

When attempting to generalize this result to other stations, we obtained only mediocre results. In the near field (COCO, DGAR), the high-frequency components of the tsunami interfere with seismic mantle waves from the large aftershock at 04:21 in the Nicobar Islands. At larger distances, the amplitudes decay rapidly, as a result of the strong dispersion under the deep water regime. Even at CRZF, a volcanic island generally similar in structure to Amsterdam, little energy is present above 2.5 mHz. At the continental coastal station CASY, most of the energy is concentrated below 2 mHz, and the large continental shelves probably act as low-pass filters at MSEY and DRV, where the energy in the tsunami signals falls off rapidly above 1.5 mHz.

4. Quantification of the Seismic Records of the Tsunami

In order to interpret the seismic records of the tsunami, we concentrate on their low-frequency components, typically in the 0.3–1.5 mHz range, and note that at such periods, the receiving stations are generally within one wavelength of the abyssal plain where most of the propagation takes place. We then make the extreme simplifying assumption that the shoreline seismometer actually functions as a horizontal Ocean-Bottom Seismometer (OBS), simply attached to the solid Earth structure underlying the water column in an unperturbed abyssal plain. Following the seminal work of WARD (1980), it has long been known that the tsunami eigenfunction is not limited to the oceanic layer, but is prolonged into any substratum with finite rigidity μ in the form of a pseudo-Rayleigh wave in which potential energy is mostly elastic, as opposed to gravitational in the fluid (OKAL, 2003). While boundary conditions predict a discontinuity of the horizontal component of particle displacement at the ocean bottom, the latter does not vanish in the elastic medium, where its expression can be obtained in the limit $\omega \rightarrow 0$ as

$$l\, y_3 = \frac{1}{4} \cdot \frac{\eta \rho_w g}{\mu k} \tag{2}$$

using the formalism of OKAL (1988, 1991, 2003) and the notation of SAITO (1967); η is the vertical amplitude of the eigenfunction y_1 at the surface of the ocean, and ρ_w the density of the ocean water.

In addition, we note following GILBERT (1980) that a horizontal seismometer responds to a spheroidal mode of the Earth through the combination of its horizontal displacement, of the tilt component of the strain induced by the passage of the equivalent wave, and of a component of gravity anomaly. As fully discussed in the Appendix, the effect of the latter two is usually negligible, at most marginal, for seismic modes, but will become primordial for a tsunami mode.

We rewrite GILBERT's (1980) equation (4.13)

$$AV = \omega^2 V - r^{-1} l\, (gU + \Phi) \tag{3}$$

in the formalism of SAITO (1967) as an apparent horizontal component y_3^{app} of the tsunami eigenfunction by noting that $ly_3 = V$; $y_1 = U$; and $y_5 = -\Phi$, and obtain

$$y_3^{app} = y_3 - \frac{1}{r\omega^2} \cdot (g y_1 - y_5), \tag{4}$$

where the $\{y_i\}$ make up the solution's eigenvector, $l = ka$ is the angular order of the equivalent normal mode (a being the radius of the Earth), and $r \approx a$ the radius at the recorder.

We further assume that the tsunami is simply excited by a point source double-couple, of seismic moment M_0 with strike, dip and slip angles ϕ_f, δ and λ, with the receiver at distance Δ and azimuth ϕ_s, and detail the computation in the

case of the record at Casey, Antarctica (CASY) shown on Figure 2. After deconvolution of the instrument response, we measure spectral amplitude peaks $X(\omega) = 4000$ cm*s at $T = 840$ s and $X(\omega) = 4700$ cm*s at $T = 1175$ s (Fig. 5). We present below a detailed analysis of the former measurement. Note that such spectral amplitudes are at least one order of magnitude greater than those expected from the Earth's free oscillations in a corresponding range of frequencies (STEIN and OKAL, 2005).

We first proceed to compute the eigenfunction of the equivalent tsunami normal mode at this period, using an Earth model derived from PREM (DZIEWONSKI and ANDERSON, 1981) and featuring an ocean of depth $H = 4$ km, the corresponding angular order being $l = 242$. Using $\eta = 1$ cm as a normalization of the vertical displacement at the free surface, we obtain a vertical displacement of the ocean bottom $y_1 = -3.12 \times 10^{-2}$ cm, an overpressure at the sea floor $-y_2 = 974$ dyn/cm^2, a horizontal component of the eigenfunction at the sea floor $y_3 = 4.12 \times 10^{-6}$ cm in the solid Earth and 2.72×10^{-2} cm in the fluid column, and a potential component of the eigenfunction, $y_5 = 0.946$ cm^{2}s^{-2}. The values of y_1 and y_3 are also in good agreement with those predicted (-2.77×10^{-3} and 3.81×10^{-6} cm, respectively) under the asymptotic approximations derived for an ocean layer over a homogeneous half

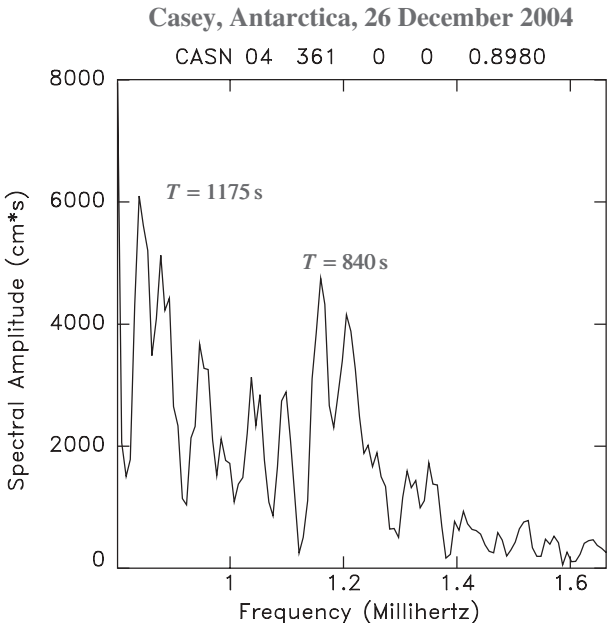

Figure 5
Spectral amplitude of the deconvolved apparent ground motion at CASY.The measurement of the spectral peaks allows the resolution of the seismic moment of the source. See text for details.

space by OKAL (2003). These numbers combine to an apparent horizontal eigenfunction $y_3^{app} = 1.17 \times 10^{-4}$ cm in (3), where the tilt term (0.85×10^{-4} cm) is predominant. Conversely, this suggests, for the CASY record, a spectral amplitude of the vertical displacement of the tsunami wave at the surface $\eta(\omega) = X(\omega)/(l \times y_3^{app}) = 1.42 \times 10^5$ cm*s.

From this spectral amplitude $\eta(\omega)$, we can obtain an estimate of the seismic moment M_0 of the earthquake using the M_{TSU} algorithm introduced by OKAL and TITOV (2007). We recall that this procedure parallels that of the mantle magnitude M_m developed by OKAL and TALANDIER (1989), and is derived from the representation of the tsunami wave as a branch of normal modes of the Earth (WARD, 1980). In this formalism, for $T = 840$ s, the source correction is $C_S^{TSU} = 2.201$, and at $\Delta = 74.2$ degrees, the distance correction is $C_D = -0.008$. We then obtain $M_{TSU} = \log_{10} \eta(\omega) + C_D + C_S^{TSU} + 3.10 = 10.44$, equivalent to a seismic moment $M_0 = 2.75 \times 10^{30}$ dyn*cm. A more rigorous calculation correcting for the exact excitation of the mode for the particular focal geometry and azimuth of the receiver, rather than using C_S^{TSU}, leads to $M_0 = 1.56 \times 10^{30}$ dyn*cm for the Harvard CMT centroid depth $h = 29$ km. For the second spectral peak ($T = 1175$ s; $l = 172$; $X(\omega) = 4700$ cm*s, one finds similarly $M_{TSU} = 10.30$, and $M_0 = 1.21 \times 10^{30}$ dyn*cm when using the exact source geometry.

Given the many approximations involved in this computation, namely that the seismometer functions as an OBS in the absence of the continental structure, and that the rupture can be modeled as a point source double-couple, we regard the agreement between our estimates and those resulting from seismological inversions ($M_0 = 1.0 \times 10^{30}$ dyn*cm (STEIN and OKAL, 2005); $M_0 = 1.15 \times 10^{30}$ dyn*cm (TSAI *et al.*, 2005) as remarkable. Certainly, these calculations reproduce an excellent order of magnitude of the exceptional size of the earthquake. In Table 1

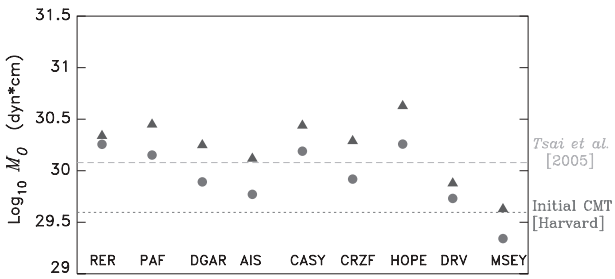

Figure 6
Estimates of the seismic moment of the 2004 Sumatra earthquake obtained from spectral amplitudes recorded at nine seismic stations, using the M_{TSU} algorithm (triangles) or a more exact correction for source geometry (circles). The dotted line represents the moment initially inverted by the Harvard CMT project, and the dashed one the full moment of the composite source inverted by TSAI *et al.* (2005). The deficient values at DRV and MSEY express the effect of their extended continental shelves.

and Figure 6, we extend our measurements to eight additional stations. At each station, the moment is measured at the period featuring the spectral amplitude of horizontal ground displacement with highest signal-to-noise ratio in the range 500–5000 s; in practice these periods vary from 800 to 3000 seconds. We exclude stations such as Bermuda and Scott Base for which the tsunami path around continental masses departs significantly from a great circle. We also do not process the record at Cocos Island, on which the timing of the arrivals is difficult to reconcile with a definitive path, as already noted by YUAN *et al.* (2005). If we further exclude the clearly deficient results at MSEY (Mahé, Seychelles) and DRV (Dumont d'Urville, Antarctica), the geometrically averaged values of the moments are 2.29 and 1.16×10^{30} dyn*cm, using the M_{TSU} and full correction algorithms, respectively, or only 0.30 ± 0.15 and 0.00 ± 0.18 logarithmic units over TSAI *et al.*'s (2005) solution (dashed line on Fig. 6). In particular, all these measurements suggest a moment several times larger than the original Harvard CMT solution of 3.95×10^{29} dyn*cm (dotted line on Fig. 6). They also confirm that the amplitude of the tsunami in the far field is well accounted for by conventional mechanisms of generation (once the exceptional size of the seismic moment is recognized), and discount the need for ancillary mechanisms of excitation (influence of steep slopes in the epicentral area; contribution of splay faults; large landslides).

We interpret the significant deficiencies of the solutions at MSEY, and to a lesser extent at DRV, as site effects. Even though MSEY is within 2 km of the shoreline, the Seychelles Islands have a continental structure (WEGENER, 1915; DU TOIT, 1937; DAVIES, 1968), whose shelf extends about 120 km at sea in the direction of arrival of the tsunami. Thus, the station cannot be regarded as coastal, let alone as functioning as an OBS. Similarly, the extended continental shelf seaward of DRV is probably responsible for the damping of the tsunami signal at this otherwise coastal station.

We similarly attempted to invert a seismic moment from the spectral amplitudes of the high-frequency components of the tsunami recorded at AIS, and described in Section 2. We use the full source correction, since the the M_{TSU} algorithm should not be used at such periods, as the modeling of the correction C_{TSU} was carried out only in the 0.3–4 mHz frequency range (OKAL and TITOV, 2006). For amplitudes $X(\omega) \approx 500$ and 1000 cm*s at the principal spectral peaks ($T = 160$ and 200 s), we obtain $M_0 = 6.2$ and 3.4×10^{29} dyn*cm, respectively. These values, especially the second one, underestimate the moment of the event. We attribute this deficiency to the significant depth extent of the source, for which the model of a point source, legitimate at low frequencies ($\sim$1 mHz), becomes increasingly simplistic at 5–10 mHz, this effect being directly comparable to the deficiency affecting conventional surface wave magnitudes M_S when the source depth becomes comparable to the wavelength.

5. Application to Other Events

The purpose of this section is to apply the above formalisms to a selection of other tsunamigenic earthquakes, in order to confirm the universal character of seismic recordings of tsunamis, and to explore any possible quantitative correlation between their amplitudes and the size of the parent earthquakes. All relevant information is summarized in Table 3.

• *The "Second" Sumatra (Nias) Earthquake of 28 March 2005*

Although damaging in the near field, the tsunami generated by this earthquake was deceptively small in the far field, a reflection of the shallow waters and large islands present in the rupture area (SYNOLAKIS and ARCAS, quoted by KERR, 2005). Nevertheless, YUAN *et al.* (2005) did mention a seismic recording at DGAR. We were able to detect the tsunami on seismic records at at least eight stations, listed in Table 3, and to make spectral measurements at DGAR and CRZF (at the other stations, the spectrum does not exhibit an appropriate signal-to-noise ratio). While the seismic moment inverted from these records remains large, it definitely characterizes the Nias earthquake as smaller than the 2004 Sumatra-Andaman one.

There are, however, significant differences between the seismic recordings of the two Sumatra tsunamis. The 2005 tsunami was not recorded above noise level at the Antarctic stations (CASY, DRV, SBA), and its record featured prominent ultra-long period instabilities at MSEY. High-frequency components are not detected at Amsterdam Island. Perhaps most astonishing is the timing of the signal at KIP, around 15:20 on 29 March, or only 23 hours after origin time (Fig. 7), which would correspond to eastward propagation, south of Australia, into the Tasman Sea and the Southwest Pacific, rather than westward through the Drake Passage on 26 December, 2004. We have no explanation for this difference in routing between the two tsunamis.

• *The Peruvian Tsunami of 23 June 2001*

This tsunami was damaging in the near field (OKAL *et al.*, 2002), while its parent earthquake was at the time the largest in the CMT catalogue ($M_0 = 4.7 \times 10^{28}$ dyn-cm), which it remained until the 2004 Sumatra earthquake. As shown on Figure 7a, the tsunami is well recorded in the South central Pacific, from Pitcairn to Rarotonga. Spectral measurements at RAR and PPT give an average moment only 11% larger than the Harvard CMT solution.

The 2001 Peruvian tsunami was also recorded by the H2O observatory (CHAVE *et al.*, 2002) which operated on the ocean bottom about half way between Hawaii and the Pacific Coast of the US from 1999 to 2003. The tsunami can be identified in the spectrogram of the horizontal long-period component oriented N168°E

Table 3

Characteristics of seismic records from other tsunamis, 1995–2006

Station		Epicentral distance (km)	Arrival date and time	Prominent component	Prominent period (s)	Apparent ground motion		Inverted seismic moment M_0 (dyn*cm)
Code	Location					Peak-to-peak (cm)	Spectral amplitude $X(\omega)$ (cm*s)	
Nias (Indonesia), 28 MAR (087) 2005; 16:10:32 UT; 1.67°N; 97.07°E; $M_0 = 1.05 \times 10^{29}$ dyn*cm								
DGAR	Diego Garcia, BIOT	2911	(087) 20:16	EW	800	9.2	800	1.99×10^{29}
MSEY	Mahé, Seychelles	4674	(087) 23:12	N247E	2500	1.0		
AIS	Ile Amsterdam, TAAF	4815	(087) 22:43	EW	2500	1.7		
RER	Rivière de l'Est, Réunion Is.	5157	(087) 22:25	EW	2900	0.5		
PAF	Port-aux-Français, Kerguelen, TAAF	6220	(088) 01:20	NS	2600	1.8		
CRZF	Ile de la Possession, Crozet Is., TAAF	6925	(088) 01:52	EW	1000	1.0	800	1.81×10^{29}
					1250		1100	1.97×10^{29}
HOPE	Hope, South Georgia	12815	(088) 10:10	NS	3200	2.2		
KIP	Kipapa, Hawaii, USA	17000 (*)	(088) 15:20	NS	3000	0.16		
Peru, 23 JUN (174) 2001; 20:33:14 UT; 17.28°S; 72.71°W; $M_0 = 4.7 \times 10^{28}$ dyn*cm								
PTCN	Pitcairn Is., B.C.C.	5917	(175) 04:57	EW	800	1		
PPT	Papeete, Tahiti, Fr. Polynesia	8092	(175) 07:56	N5E	1100	0.3		
RAR	Rarotonga, Cook Is.	8977	(175) 09:01	N335E	800	0.3	200	6.05×10^{28}
					1000		300	6.72×10^{28}
					1550		250	3.50×10^{28}
H2O	Hawaii-2 Observatory	8978	(175) 09:13	N168E				
Antofagasta (Chile), 30 JUL (211) 1995; 05:11:57 UT; 24.17°S; 70.74°W; $M_0 = 1.2 \times 10^{28}$ dyn*cm								
RPN	Easter Island, Chile	3870	(211) 10:35	NS	690	0.3	100	2.87×10^{28}

Table 3

(Contd.)

Station		Epicentral distance (km)	Arrival date and time	Prominent component	Prominent period (s)	Apparent ground motion		Inverted seismic moment M_0 (dyn*cm)
Code	Location					Peak-to-peak (cm)	Spectral amplitude $X(\omega)$ (cm*s)	
RAR	Rarotonga, Cook Is.	8972	(211) 17:45	NS	800	0.3	70	2.18×10^{28}
KIP	Kipapa, Hawaii, USA	10699	(211) 20:09	NS	1750	0.2	250	3.37×10^{28}
Biak (Indonesia), 17 FEB (048) 1996; 05:59:30 UT; 0.67°S; 136.62°E; $M_0 = 2.4 \times 10^{28}$ dyn*cm								
GUMO	Agaña, Guam	1823	(048) 08:31	NS	1000	0.3	150	2.08×10^{28}
ERM	Erimo, Japan	4781	(048) 12:43	NS	1000	0.9		
Tonga, 03 MAY (123) 2006; 15:27:09 UT; 20.33°S; 174.03°W; $M_0 = 9.6 \times 10^{27}$ dyn*cm								
PTCN	Pitcairn Is., B.C.C.	6564	(123) 21:29	NS	690	1.4		
KIP	Kipapa, Hawaii, USA	4944	(123) 22:23	NS	1400	0.07	200	4.27×10^{28}
RPN	Easter Island, Chile	6564	(124) 00:37	NS	690	0.2	125	3.57×10^{28}

(*) Distance estimated along off-great circle path going south of Australia.

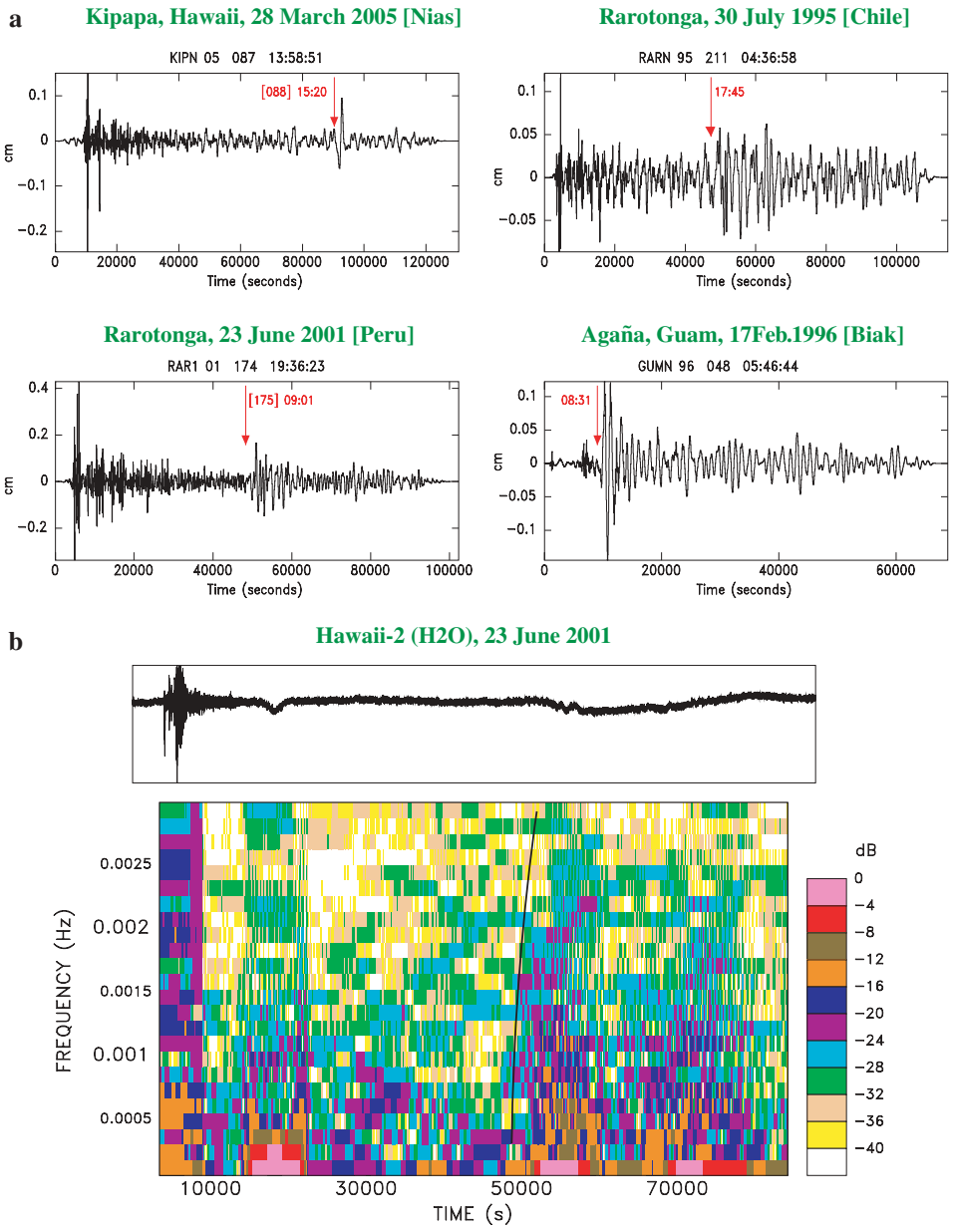

Figure 7

(**a**) Examples of seismic recordings of tsunamis from smaller earthquakes. The arrows identify the arrival of the tsunami at selected stations. These records represent apparent ground motion (in cm) after instrument deconvolution and bandpass filtering between 0.1 and 10 mHz. (**b**) Time series and spectrogram at the ocean-bottom observatory H2O following the 2001 Peruvian earthquake. The black line across the spectrogram shows the expected arrival of the tsunami, dispersed according to (1); note the coherent increase in spectral density, but the following nonlinearity in the record, probably triggered by the passage of the tsunami.

(Fig. 7b), on the basis of the coherent rise in spectral density between 0.3 and 2 mHz at the group arrival times predicted by the dispersion relation (1). However, the record suffers from obvious nonlinearity following this arrival and cannot be processed quantitatively; it is possible that this instability was triggered by the tsunami. Under the shallow water approximation, the ratio of velocity of horizontal flow V in the water column to vertical surface displacement η is simply $V/\eta = \sqrt{g/H}$, which predicts V on the order of a few mm/s. It is unclear whether this would suffice to disturb the loose sedimentary structure in which the instrument at H2O was deployed. Also, we note another occurrence of similar instability much earlier in the time series.

• *The Antofagasta, Chile Tsunami of 30 July 1995*

This was the last Pacific tsunami with reported damage in the far field, as it rocked a supply ship against the bottom of the harbor of Hakahau on Ua Pou in the Marquesas Islands (GUIBOURG *et al.*, 1997). The tsunami is well recorded on seismic instruments from Easter Island to Western Samoa; however the record at AFI is affected by strong nonlinearity. The average moment measured from spectral amplitudes, $M_0 = 2.7 \times 10^{28}$ dyn-cm, is about 2.3 times the CMT solution.

• *The Biak, Indonesia Tsunami of 17 February 1996*

This large earthquake ($M_0 = 2.4 \times 10^{28}$ dyn*cm) generated a locally devastating tsunami which caused at least 120 deaths (MATSUTOMI *et al.*, 2001), but was recorded only marginally in the far field. We were able to identify a seismic recording of the tsunami at Station GUMO (Agaña, Guam), where the spectral amplitude (150 cm*s at 1 mHz) leads to an excellent value of the seismic moment (2.08×10^{28} dyn*cm). Unfortunately, Station KIP in Hawaii was down at that time.

• *The Tonga Tsunami of 03 May 2006*

We also consider the case of this recent event, reminiscent of the 1977 intraslab Tonga earthquake (TALANDIER and OKAL, 1979; LUNDGREN and OKAL, 1988), 300 km to the South. Despite a relatively deep focus (65 km), the tsunami is detectable at seismic stations PTCN, RPN and KIP (at the time of writing, not all South Pacific stations are available), and spectral amplitudes could be quantified at the latter two.

These results are summarized on Figure 8, which compares seismic moments inverted from spectral amplitudes of seismic recordings of the tsunamis to the Harvard CMT solutions. This figure suggests a remarkable correlation, at least for $M_0 \geq 2 \times 10^{28}$ dyn*cm, which serves to justify *a posteriori* the many assumptions used in the present approach. It also confirms that the 2004 Sumatra earthquake was not

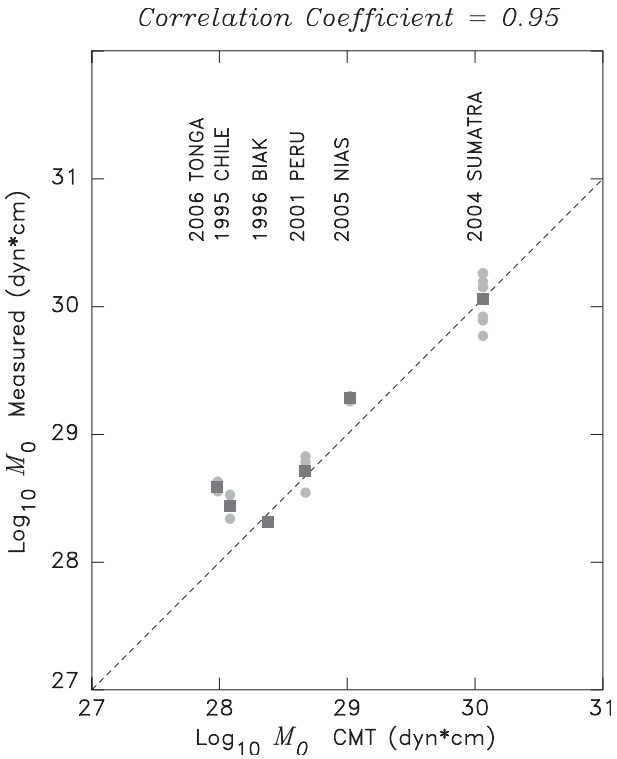

Figure 8
Comparison of moments retrieved from spectral amplitudes of seismic records of six tsunamis with published CMT solutions. For each earthquake, the gray circles are measurements at individual stations (analogous to the circles on Fig. 6), and the squares the resulting geometrical average of the moments. In the case of the 2004 Sumatra event, the deficient values at MSEY and DRV have been excluded.

anomalously tsunamigenic, and reconciles the amplitude of its tsunami with its seismic source.

Finally, we examined the case of the Papua New Guinea tsunami of 17 July 1998. The tsunami was catastrophic in the near field, with run-up reaching 15 m and causing 2200 deaths, and is generally interpreted as resulting from an underwater landslide triggered by the earthquake with a delay of 13 minutes (SYNOLAKIS *et al.*, 2002). Figure 9 shows that the tsunami is detectable on the EW component of the regional station GUMO, between 1.5 and 3.5 mHz, with a dispersion of group times suggesting propagation over an average water depth of 3 km, generally compatible with the bathymetry of the shallow Eauripik Rise separating the East and West Caroline Basins. However, the peak spectral amplitudes on this record ($X(\omega)$ = 30 cm*s at T = 690 s and 2.5 cm*s at T = 330 s) lead to seismic moments of 6.1×10^{27} and 1.29×10^{28} dyn*cm, or 16 and 35 times the Harvard CMT solution,

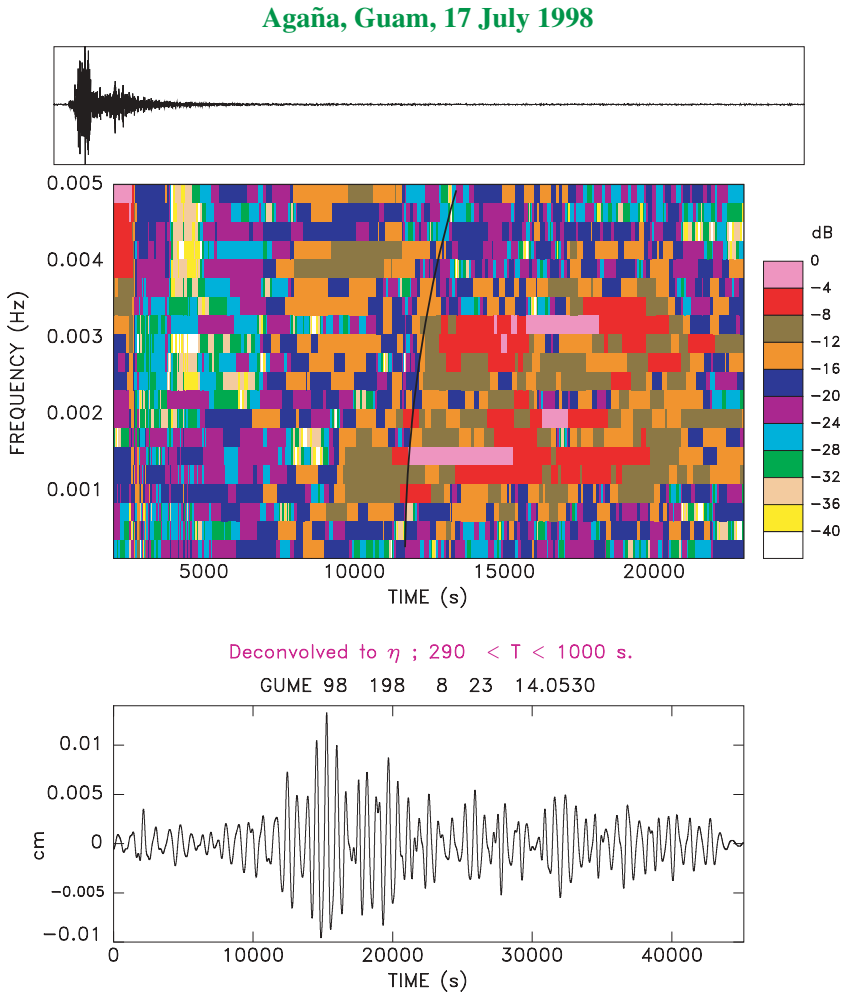

Figure 9

Top: Time series of the EW long-period channel at Agaña, Guam (GUMO) following the Papua New Guinea earthquake of 17 July, 1998. The record is 25,000 s (≈ 7 hr) long. Center: Corresponding spectrogram, showing arrival of tsunami ~12,000 s into the time series with energy concentrated in the 1.2 to 3.5 mHz range. The black curve is the theoretical dispersion for propagation over a 3-km deep basin from a source located at the Sissano amphitheater and and activated at 09:02 UTC (SYNOLAKIS *et al.*, 2002). *Bottom*: Equivalent surface wave amplitude η deconvolved from the top trace following the procedure in Section 6, but bandpass filtered between 290 and 1000 s.

respectively. This confirms, if need be, that the 1998 Papua New Guinea tsunami could not have been generated directly by the main shock. These observations represent to our knowledge the first detection of the 1998 Papua New Guinea

tsunami at a distance (1809 km) falling outside the near field domain, which can be used to support this conclusion.

6. Deconvolution of the Seismic Records

In this section, we explore the possibility of deconvolving the response of the seismometer to the tsunami in order to reconstruct the time series of the surface displacement of the tsunami wave, $\eta(t)$. For this purpose we define at each frequency a so-called "Gilbert Response Factor" $GRF(\omega) = ly_3^{app}$, which is just the ratio between the apparent ground motion "felt" by the seismometer (still supposed to reside on the ocean bottom) and the vertical displacement of the surface of the ocean (normalized to unity in our computations of eigenfunctions). This function is simply

$$GRF(\omega) = l \cdot y_3^{app} \approx ly_3 - \frac{1}{C\,\omega}(gy_1 - y_5), \tag{5}$$

where C is the phase velocity of the wave, and we have further assumed that the depth of the ocean column is negligible with respect to the Earth's radius a. $GRF(\omega)$ is readily computed from normal mode theory, and Figure 10 shows its variation over a wide range of frequencies both within and outside the shallow-water approximation ($lH/a \ll 1$). We verified (see Appendix) that for a given frequency, $GRF(\omega)$ depends only marginally on the depth of the ocean column. We then simply divide, in the Fourier domain, the apparent seismic amplitude $X(\omega)$ by

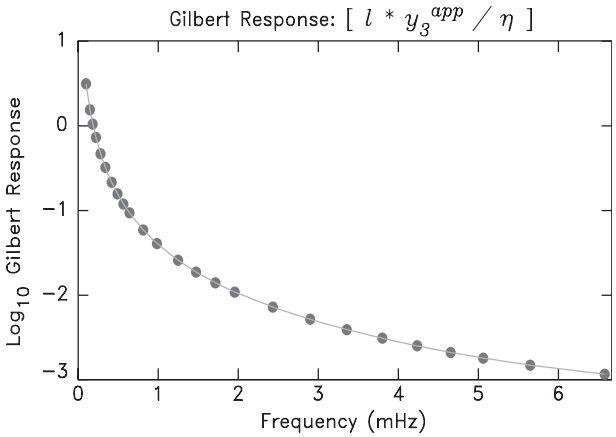

Figure 10
"Gilbert Response Factor" as a function of frequency computed for a 5-km deep ocean. At each frequency, *GRF*, defined by (5), represents the ratio between the apparent displacement to which a horizontal seismometer on the ocean bottom responds and the vertical amplitude of the tsunami wave on the surface of the ocean.

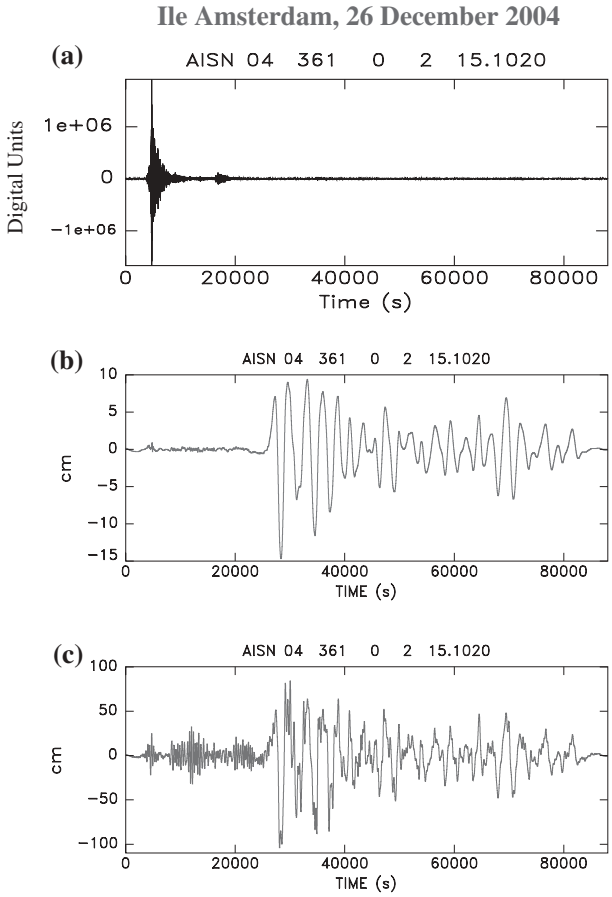

Figure 11
Reconstruction of the tsunami wave time series from a seismogram by deconvolution of the Gilbert Response Factor *GRF*, illustrated on the example of Station AIS (2004 Sumatra event). (*a*): Raw Long-period NS seismogram at AIS; (*b*): Apparent horizontal ground motion after instrument deconvolution and bandpass filtering between 0.1 and 10 mHz; (*c*): Reconstructed time series of the sea surface deformation, η.

$GRF(\omega)$ before returning to the time domain to reconstruct the time series $\eta(t)$ of the tsunami at the surface. This procedure is illustrated on Figure 11 in the case of the record at Amsterdam Island (AIS). The top frame shows the raw record, the middle one the time series of the apparent ground displacement after removing the instrument response and bandpass filtering between 100 and 10000 s, and the bottom one the time series resulting from the deconvolution of the Gilbert Response Factor, and further filtering between 300 and 5000 s. In the framework of our admittedly crude assumptions, this record should in principle represent the

time series of the wave elevation $\eta(t)$ of the surface of the ocean at the location, but in the absence, of Amsterdam Island. Obviously, the high-frequency signal to the left of the tsunami in the deconvolved trace should be ignored, as it represents the result of processing the seismic surface waves from the earthquake through an algorithm which is not applicable to them. This procedure was carried out for all 16 seismic records of the tsunami and the results, expressed as peak-to-peak η, are listed in Table 1.

Unfortunately, no instruments capable of directly recording the 2004 Sumatra tsunami on the high seas were operating at the time in the Indian Ocean, and thus it is impossible to compare the results of our deconvolution to the actual height of the tsunami. We nevertheless validate our algorithm in three different ways. First, we use the record of the tsunami obtained by the JASON satellite altimeter which featured a zero-to-peak amplitude of ~70 cm (SCHARROO *et al.*, 2005), on the same order of magnitude as the deconvolved time series η on Figure 11 (85 cm). We emphasize, however, the strong limitations of this comparison, given that the JASON trace is neither a time nor a space series, and that it samples the tsunami several thousand km to the north of AIS.

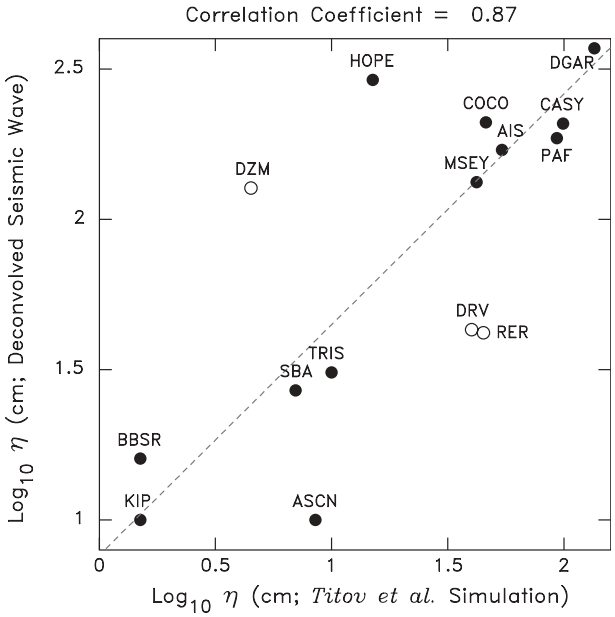

Figure 12
Equivalent tsunami wave height η deconvolved from seismic records (ordinate) plotted against the wave height computed from TITOV *et al.*'s (2005) global simulation of the 2004 Sumatra tsunami. The open symbols are outliers excluded from the regression; see text for details. The dashed line is the best-fitting regression to the dataset.

►

Figure 13

Analysis of the seismic record of the 2006 Tonga tsunami at Kipapa, Hawaii. (*a*): Raw record of the North-South Long-Period channel; the record starts at 14:58:29 UTC. (*b*): Spectrogram of (a), identifying the tsunami arrival, about 25,000 s into the signal. The black trace is the dispersion expected from propagation over a 4.5-km deep ocean basin. (*c*): Apparent ground motion recorded by the instrument, after deconvolution of its response. The red arrow points to the arrival of the tsunami, barely discernible above noise level, but clearly present in the spectrogram. The time scale is common to (a), (b) and (c). (*d*): Surface wave height, η, reconstructed by deconvolution of the Gilbert Response Factor. (*e*): Tsunami waveforms recorded at tsunameters of the DARTprogram deployed off the islands of Oahu (DART-ETD; red trace) and Hawaii (DART-II; black trace); the scale in cm at left corresponds to equivalent tsunami height at the sea surface (Courtesy V.V. Titov).

Second, we compare in Figure 12 the peak-to-peak amplitudes of our deconvolved traces (listed in Table 1) to those computed as part of TITOV *et al.*'s (2005) global simulation of the 2004 tsunami. Specifically, for each station, we extracted from these authors' database a time series at a "virtual gauge" located on the high seas in the neighborhood of the station (typically 50 km out at sea, but with allowances made for exceptional structures), and retained its peak-to-peak amplitude, which we list as the last column of Table 1. The dataset is well correlated, except for a number of intriguing outliers. Among them is Dumont d'Urville (DRV), where we have already noted the deficient amplitude of the tsunami signal, possibly due to the large continental shelf bordering the continent; the virtual gauge is located seaward of the shelf. Both DZM in New Caledonia and RER in Réunion are the only stations at substantial altitude (in both cases $\sim$800 m), which may affect their response; we note however that one of them (DZM) has an enhanced response, the other (RER) a deficient one. Excluding those three stations, we find a very strong correlation (87%) between our deconvolved amplitudes and those simulated by TITOV *et al.* (2005). However, we have no interpretation for the extreme amplitude deconvolved at HOPE (although it may express some form of resonance of the strongly indented Cumberland Bays where the station is located), nor for the extreme deficiency at Ascension Island (ASCN). Also, we note that, while the deconvolved amplitudes correlate with the simulated ones, the former remain generally several times larger than the latter.

Finally, we take advantage of the recent deployment of many tsunameters (GONZÁLEZ *et al.*, 2005), notably in the Pacific Basin, to compare the deconvolved wave height of the Tonga tsunami of 03 May 2006 recorded at Kipapa, Hawaii, with time series obtained at two nearby tsunameters. As shown in Figure 13, and while significant differences remain between the waveshapes involved, the peak-to-peak amplitude deconvolved in our experiment, 1.6 cm, is comparable to that (2.1 cm) recorded at the offshore site DART-ETD, approximately 110 km from Station KIP, the ratio of these amplitudes (0.76), being itself comparable to the scatter (0.79) between the amplitudes at the two tsunameters.

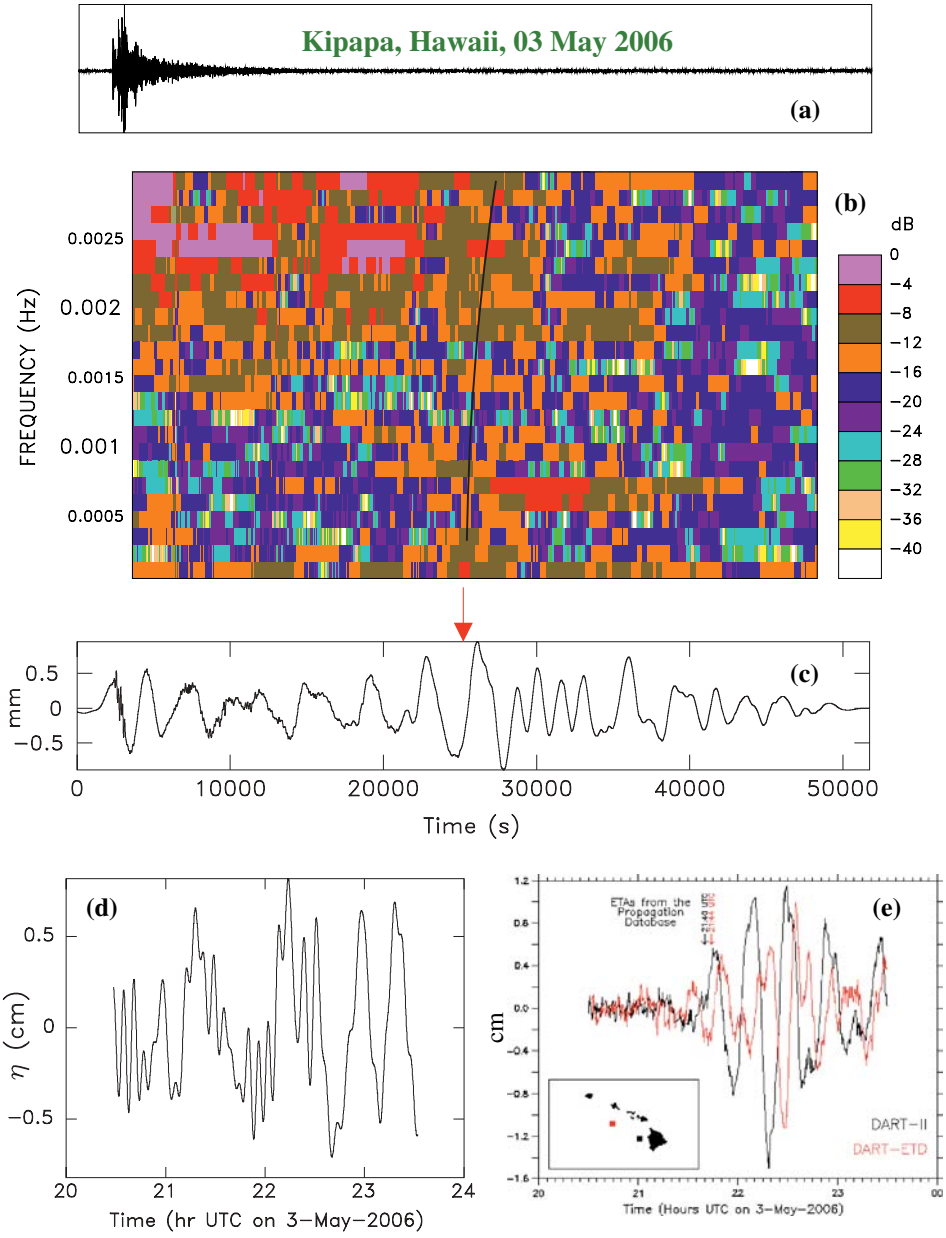

7. Conclusion and Perspective

We have expanded the observations of YUAN *et al.* (2005) and HANSON and BOWMAN (2005), and established that the 2004 Sumatra earthquake was recorded

essentially worldwide on the horizontal long-period channels of seismic stations located in the vicinity (within ~35 km) of shorelines. However, the recording can be affected by site effects such as the presence of an extended continental shelf; large bays can apparently enhance the signal (as at HOPE), or suppress it (as at ATD). At intermediate ranges of distance (~4000 km), we show that seismometers can detect the full spectrum of a tsunami branch, including their higher-frequency component up to 10 mHz, which are strongly affected by dispersion outside the domain of applicability of the shallow water approximation.

We have shown that it is possible to interpret seismic recordings of the tsunami as representing the response of the seismometer to a deformation of the ocean floor involving lateral displacement, tilt and gravitational potential, as derived theoretically by GILBERT (1980). In this model, it is assumed that, for stations located much closer to the shoreline than one wavelength, the progressive wave is essentially unaltered from its structure on the high seas, with the result that the instrument functions as an Ocean-Bottom Seismometer responding to the tsunami in a deep basin. Estimates of the seismic moment of the parent earthquake obtained in this framework and using standard normal mode theory (WARD, 1980; OKAL, 1988, 2003) are in excellent agreement with published values, which serves to justify the model, however outrageous the approximations involved may sound.

In addition, we show that tsunami signals are present in the seismic recordings of at least five more earthquakes, and that the seismic moments derived from our algorithm scale remarkably well with published centroid-moment tensor values.

The technique can be extended to a formal deconvolution of the seismic records by removal of the Gilbert Response Function. On Figures 12 and 13, we found a clear correlation between the amplitudes of the resulting time series and those obtained from TITOV *et al.*'s [2005] global simulation (and in one case with a genuine tsunameter record). This further confirms that such deconvolved signals are representations of the tsunami wavefields on the high seas, and hence supports the validity of the interpretation of the seismic recordings of the tsunamis. While this requires a number of drastic simplifying assumptions, and notwithstanding the potential importance of site effects at individual locations, the seismic instruments have the great advantage of being for the most part already deployed on many oceanic islands and continental shores, and in any case of coming at a fraction of the deployment and above all maintenance costs of a network of bottom pressure recorders linked to their open-seas buoys. The present study suggests that existing or future broadband horizontal seismometers located near shore on oceanic islands or continents could complement advantageously a network of buoy-based instruments of the DART type.

Acknowledgments

This research was supported by the National Science Foundation, under Grant CMS-03-0154. I thank Rainer Kind for many discussions on this and other topics in Potsdam in the Fall of 2005. I am grateful to Vasily Titov for access to the database of global simulations of the Sumatra tsunami (TITOV *et al*., 2005), and for the DART tsunameter records included in Figure 13. I thank Steve Ward for his review of the original version of the paper, and in particular for his suggestion to look at vertical records. Figure 1 was plotted using the GMT software (WESSEL and SMITH, 1991).

Appendix

Tilt and Gravity Terms Compared for Seismic and Tsunami Modes

We compare here the various contributions from displacement, tilt and gravity to the recording by long-period seismometers, of conventional seismic and tsunami modes.

In addition to the response of a horizontal seismometer, given by equations (3) or (4), we consider GILBERT'S (1980) expression for the response of a vertical seismometer (his equation (4.12) p. 66):

$$AU = \left(\omega^2 + \frac{2g}{r}\right)U + \frac{l+1}{r}\Phi, \tag{A-1}$$

which we rewrite in the formalism of SAITO (1967) as equivalent to the recording of an apparent vertical displacement y_1^{app}

$$y_1^{app} = y_1 + \frac{2g}{r\omega^2}y_1 - \frac{l+1}{r\omega^2}y_5. \tag{A-2}$$

- For conventional seismic spheroidal modes, the second terms in (4) and (A-2) are negligible as long as their period T remains less than $2\pi\sqrt{a/2g} \approx 1$ hr, which is the case of all mantle waves. As the latter carry very little gravitational energy, the third terms are also negligible and for all practical purposes, $y_1^{app} = y_1$; $y_3^{app} = y_3$; the seismometer responds to ground motion. For the lowest frequency modes, whose period approaches one hour, the contributions of the second and third terms in (A-2) become important; however, because their signs are generally opposite, the departure of y_1^{app} from y_1 does not exceed 20% (for ${}_0S_2$), as

documented in GILBERT'S (1980) Table 1 (p. 66) or DAHLEN and TROMP'S (1998) Table 10.1 (p. 375); the horizontal response would be affected more significantly for the four gravest spheroidal modes, down to ${}_0S_5$. Since few studies of the fundamental spheroidal modes are conducted on horizontal instruments, and toroidal modes are unaffected by such terms (GILBERT, 1980), the conclusion is that tilt and gravity terms contribute marginally if at all to the recording of conventional seismic modes. They do not affect the *order of magnitude* of the recorded amplitude (this would happen only in the case of the yet-to-be observed Slichter mode ${}_1S_1$).

- We illustrate the case of tsunami modes by considering a typical period of 1014 seconds, corresponding to $l = 200$ for an ocean depth of 4 km, overlying a solid Earth inspired from PREM (DZIEWONSKI and ANDERSON, 1981). For a normalization of the eigenfunction $\eta = 1$ cm at the surface of the ocean, we compute at the ocean bottom $y_1 = -0.0037$ cm; $y_3 = 5.96 \times 10^{-6}$ cm in the solid; and $y_5 = 0.0117$ (cm/s)^2. (Note that a negative value of y_1 is expected, as it expresses the downward vertical response of the elastic Earth to the overpressure accompanying an upwards vertical displacement of the ocean surface.) In turn, these numbers lead to a free air contribution (second term in (A-2)) of -2.98×10^{-4} cm (or only 8% of y_1), and to a potential contribution (third term in (A-2)) of -9.66×10^{-3} cm (or 2.6 times y_1), the apparent displacement for a vertical seismometer being ${y_1}^{app} = -0.0137$ cm. For the horizontal component, the tilt contribution to ${y_3}^{app}$ (second term in (4)) is 1.49×10^{-4} cm (25 times y_3) and the potential contribution (third term in (4)) is 4.81×10^{-5} cm (8 times y_3), for a total $y_3 = 2.03 \times 10^{-4}$ cm, and an apparent displacement $l\ {y_3}^{app} = 4.06 \times 10^{-2}$ cm, i.e., three times the amplitude of the vertical signal. This factor of three is further found to vary little with frequency.

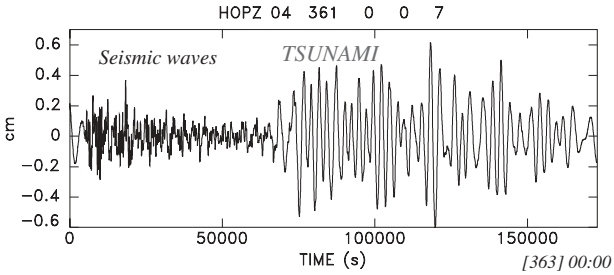

Figure A1
Deconvolved vertical record at HOPE, showing recording of the tsunami by the vertical instrument. The time window (48 hours starting at 00:00 on 26 December 2004), deconvolution and filtering are exactly analogous to those used on Figure 2 for the NS component. Note, however, that the amplitude is reduced by a factor of 10.

On Figure A1, we plot the vertical long-period seismogram at Hope, processed in exactly the same fashion as the horizontal component on Figure 2. Note that the tsunami is very prominent in this high-quality record, but that its amplitude is only 1/10 of its north-south counterpart, as opposed to the predicted 1/3. We cannot explain this discrepancy by a factor of about three, but suspect that it may be rooted in the different nature of the terms controlling the horizontal and vertical responses. The former is completely governed by the tilt term, which depends only on the wavelength of the tsunami mode, and as such may be more robust under the extreme approximation made in assuming that the island seismometer behaves as an OBS, while the vertical response is controlled principally by the potential term, for which the approximation may not hold; note in particular that the missing factor of three represents essentially the ratio y_1^{app}/y_1 at the bottom of the ocean (3.78). For this reason, we elect not to further study and attempt to quantify the vertical records of the tsunami. However, we stress that they are indeed present.

Finally, we address the question of the sensitivity of the Gilbert Response Function *GRF* to the height H of the ocean column. Under the Linear Shallow Water Approximation, we have shown in OKAL (1982, 1988) that the eigenstress y_2 at the fluid-solid interface can be taken as $y_2 = -\eta\rho_w g$, and that in turn the vertical displacement at the interface is $y_1 = y_2/Z$ with the impedance $Z = 4/3\ \mu k$ where μ is the rigidity of the substratum and k the wavenumber. As we discussed above, the *GRF* is controlled by the tilt term in (4), leading to

$$GRF = \frac{l y_3^{app}}{\eta} \approx \frac{lg}{r\omega^2} \cdot \frac{3}{4} \frac{\rho_w g}{\mu k} \approx \frac{3}{4} \cdot \frac{\rho_w g^2}{\mu} \cdot \frac{1}{\omega^2}. \tag{A-3}$$

This expression is expected to be independent of H, which we verified by recomputing all the contributions to y_1^{app} and y_3^{app} for an ocean depth $H = 5$ km, for which the new value of l at 1014 s is 179, as opposed to ($H = 4$ km; $l = 200$) used above. We find that y_3^{app} becomes 2.23×10^{-4} cm, and thus $l\, y_3^{app} = 3.99 \times 10^{-2}$ cm, a decrease of 1.7%, and for the vertical component, $y_1^{app} = -0.0139$ cm, an absolute increase of 1.3% with respect to the case of the shallower ocean. Similar numbers are also found across the frequency spectrum, and so we conclude that the effect of H on the Gilbert Response Function *GRF* is negligible given the other approximations made in this study.

REFERENCES

BEN-MENAHEM, A. and ROSENMAN, M. (1972), *Amplitude patterns of tsunami waves from submarine earthquakes*, J. Geophys. Res. *77*, 3097–3128.

CHAVE, A.D., DUENNEBIER, F.K., BUTLER, R., PETITT, R.A., Jr., WOODING, F.B., HARRIS, D., BAILEY, J.W., HOBART, E., JOLLY, J., BOWEN, A.D. and YOERGER, D.R., H2O: *The Hawaii-2 Observatory*. *In*

Science-technology Synergy for Research in the Marine Environment: Challenges for the XXIst Century (eds. L. Beranzoli, P. Favali, and G. Smriglio), Devel. Mar. Tech. Ser., *12*, pp. 83–92 (Elsevier, Amsterdam, 2002).

DAHLEN, F.A. and TROMP, J. *Theoretical Seismology* (Princeton Univ. Press, 1998, 1025 pp.)

DAVIES, D. (1968), *When did the Seychelles leave India*? Nature *220*, 1225–1226.

DU TOIT, A.L., *Our Wandering Continents*, 366 pp. (Oliver & Boyd, London, 1937).

DZIEWONSKI, A.M. and ANDERSON, D.L. (1981), *Preliminary Earth Reference Model*, Phys. Earth Planet. Inter. *25*, 297–356.

GILBERT, F., *An introduction to low-frequency seismology*. *In Proc. Intl. School Phys. "Enrico Fermi"*, *78* (eds. A.M. Dziewonski and E. Boschi), pp. 41–81 (North Holland, Amsterdam, 1980).

GONZÁLEZ, F.I., BERNARD, E.N., MEINIG, C., EBLE, M.C., MOFJELD, H.O. and STALIN, S. (2005), *The NTHMP Tsunameter network*, Natural Hazards *35*, 25–39.

GUIBOURG, S., HEINRICH, P., and ROCHE, R. (1997), *Numerical modeling of the 1995 Chilean tsunami. Impact on French Polynesia*, Geophys. Res. Lett. *24*, 775–778.

HANSON J.A. and BOWMAN, J.R. (2005), *Dispersive and reflected tsunami signals from the 2004 Indian Ocean tsunami observed on hydrophones and seismic stations*, Geophys. Res. Lett. *32*(17), L17606, 5 pp.

KERR, R.A. (2005), *Model shows islands muted tsunami after latest Indonesian earthquake*, Science *308*, 341.

LA ROCCA, M., GALLUZZO, D., SACCOROTTI, G., TINTI, S., CIMINI, G.B., and DEL PEZZO E. (2004), *Seismic signals associated with landslides and with a tsunami at Stromboli Volcano, Italy,* Bull. Seismol. Soc. Amer. *94*, 1850–1867.

LUNDGREN, P.R. and OKAL, E.A. (1988), *Slab decoupling in the Tonga arc: the June 22, 1977 earthquake*, J. Geophys. Res. *93*, 13355–13366.

MATSUTOMI, H., SHUTO, N., IMAMURA, F., and TAKAHASHI, T. (2001), *Filed survey of the 1996 Irian Jaya earthquake tsunami on Biak Island*, Nat. Haz. *24*, 199–212.

OKAL, E.A. (1982), *Mode-wave equivalence and other asymptotic problems in tsunami theory*, Phys. Earth Planet. Inter. *30*, 1–11.

Okal, E.A. (1988), *Seismic parameters controlling far-field tsunami amplitudes: A review*, Natural Hazards *1*, 67–96.

OKAL, E.A. (1991), *Erratum [to "Seismic parameters controlling far-field tsunami amplitudes: A review"]*, Natural Hazards *4*, 433.

OKAL, E.A. (2003), *Normal modes energetics for far-field tsunamis generated by dislocations and landslides*, Pure Appl. Geophys. *160*, 2189–2221.

OKAL, E.A. and TALANDIER, J. (1989), M_m*: A variable period mantle magnitude*, J. Geophys. Res. *94*, 4169–4193.

OKAL, E.A. and TITOV, V.V. (2007), M_{TSU}: *Recovering seismic moments from tsunameter records*, Pure Appl. Geophys., *164*, 355–378.

OKAL, E.A., DENGLER, L., ARAYA, S., BORRERO, J.C., GOMER, B., KOSHIMURA, S., LAOS, G., OLCESE, D., ORTIZ, M., SWENSSON, M., TITOV, V.V., and Vegas, F. (2002), *A field survey of the Camana, Peru tsunami of June 23, 2001*, Seismol. Res. Lett. *73*, 904–917.

OKAL, E.A., FRITZ, H.M., RAVELOSON, R., JOELSON, G., PANČOŠKOVÁ, P., and RAMBOLAMANANA, G. (2006a), *Field survey of the 2004 Indonesian tsunami in Madagascar*, Earthquake Spectra *22*, S263–S283.

OKAL, E.A., SLADEN, A., and OKAL, E.A.-S. (2006b), *Field survey of the 2004 Indonesian tsunami on Rodrigues, Mauritius, and Réunion Islands*, Earthquake Spectra *22*, S241–S261.

OKAL, E.A., TALANDIER, J., and REYMOND, D. (2007) *Quantification of hydrophone records of the 2004 Sumatra tsunami*, Pure Appl. Geophys. *164*, 309–323.

SAITO, M. (1967), *Excitation of free oscillations and surface waves by a point source in a vertically heterogeneous Earth*, J. Geophys. Res. *72*, 3689–3699.

SATAKE, K. (1988), *Effects of bathymetry on tsunami propagation: Application of ray tracing to tsunamis*, Pure Appl. Geophys. *126*, 28–35.

SCHARROO, R., SMITH, W.H.F., TITOV, V.V., and ARCAS, D. (2005) *Observing the Indian Ocean tsunami with satellite altimetry*, Geophys. Res. Abstr. *7*, 230 (abstract).

STEIN, S. and OKAL, E.A. (2005), *Size and speed of the Sumatra earthquake*, Nature *434*, 581–582.

SYNOLAKIS, C.E., BARDET, J.-P., BORRERO, J.C., DAVIES, H.L., OKAL, E.A., SILVER, E.A., SWEET, S., and TAPPIN, D.R. (2002), *The slump origin of the 1998 Papua New Guinea tsunami*, Proc. Roy. Soc. (London), Ser. *A 458*, 763–789.

TALANDIER, J. and OKAL, E.A. (1979), *Human perception of T waves: the June 22, 1977 Tonga earthquake felt on Tahiti*, Bull. Seismol. Soc. Amer. *69*,1475–1486.

TITOV, V.V., RABINOVICH, A.B., MOFJELD, H.O., THOMSON, R.E., and GONZÁLEZ, F.I. (2005), *The global reach of the 26 December 2004 Sumatra tsunami*, Science *309*, 2045–2048.

TSAI, V.C., NETTLES, M., EKSTRÖM, G., and DZIEWOŃSKI, A.M. (2005), *Multiple CMT source analysis of the 2004 Sumatra earthquake*, Geophys. Res. Lett. *32*(17), L17304, 4 pp.

WARD, S.N. (1980), *Relationships of tsunami generation and an earthquake source*, J. Phys. Earth *28*, 441–474.

WEGENER, A.L., *Die Entstehung der Kontinente und Ozeane* (Vieweg, Braunschweig, 1915).

WOODS, M.T. and OKAL, E.A. (1987) *Effect of variable bathymetry on the amplitude of teleseismic tsunamis: a ray-tracing experiment*, Geophys. Res. Lett. *14*, 765–768.

WESSEL, P. and SMITH, W.H.F. (1991), *Free software helps map and display data, Eos*, Trans. Amer. Geophys. Un. *72*, 441 and 445–446.

YUAN, X., KIND, R., and PEDERSEN, H. (2005), *Seismic monitoring of the Indian Ocean tsunami*, Geophys. Res. Lett. *32*(15), L15308, 4 pp.

(Received May 29, 2006, accepted July 30, 2006)